Decaying shock studies of phase transitions in MgO-SiO 2 systems: Implications for the super-Earths' interiors

R. M Bolis, G. Morard, T. Vinci, A. Ravasio, E. Bambrink, M. Guarguaglini, M. Koenig, R. Musella, F. Remus, J. Bouchet, et al.

AGU PUBLICATIONS

Geophysical Research Letters

RESEARCH LETTER

10.1002/2016GL070466

Key Points:

- Magnesium oxides phase diagrams investigated along the Hugoniots between 0.2 and 1.2 TPa with decaying shocks and optical diagnostics
- New MgO experimental melting point proposed at 0.47 ± 0.04 TPa and 9860 ± 810 K
- No evidences of phase transition have been found for $MgSiO_3$ and Mg_2SiO_4 between 0.12–0.5 TPa and 0.2–0.85 TPa, respectively

Supporting Information:

- Supporting Information S1

Correspondence to:
R. M. Bolis,
riccardo.bolis@polytechnique.edu

Citation:
Bolis, R. M., et al. (2016), Decaying shock studies of phase transitions in MgO-SiO_2 systems: Implications for the super-Earths' interiors, *Geophys. Res. Lett.*, *43*, 9475–9483, doi:10.1002/2016GL070466.

Received 18 JUL 2016
Accepted 3 SEP 2016
Accepted article online 14 SEP 2016
Published online 28 SEP 2016
Corrected 23 FEB 2018

This article was corrected on 23 FEB 2018. See the end of the full text for details.

Decaying shock studies of phase transitions in MgO-SiO_2 systems: Implications for the super-Earths' interiors

R. M. Bolis[1,2], G. Morard[3], T. Vinci[1,2], A. Ravasio[1,2], E. Bambrink[1,2], M. Guarguaglini[1,2], M. Koenig[1,2,4], R. Musella[5], F. Remus[6], J. Bouchet[6], N. Ozaki[7,8], K. Miyanishi[8], T. Sekine[9], Y. Sakawa[10], T. Sano[10], R. Kodama[4,7,8], F. Guyot[3], and A. Benuzzi-Mounaix[1,2]

[1]LULI - CNRS, Ecole Polytechnique, CEA, Université Paris-Saclay, F-91128 Palaiseau cedex, France, [2]Sorbonne Universités, UPMC Univ Paris 06, CNRS, Laboratoire d'utilisation des lasers intenses (LULI), place Jussieu, 75252 Paris cedex 05, France, [3]Institut de Minéralogie, de Physique des Matériaux et de Cosmochimie, UMR CNRS 7590, Sorbonne Universités-Université Pierre et Marie Curie, CNRS, Muséum National d'Histoire Naturelle, IRD, Paris, France, [4]Institute for Academic Initiatives, Osaka University, Suita, Japan, [5]LUTH, Observatoire de Paris, CNRS, Université Paris Diderot, Meudon, France, [6]CEA, DAM, DIF, Arpajon, France, [7]Graduate School of Engineering, Osaka University, Suita, Japan, [8]Photon Pioneers Center, Osaka University, Suita, Japan, [9]Department of Earth and Planetary Systems Science, Hiroshima University, Higashihiroshima, Japan, [10]Institute of Laser Engineering, Osaka University, Suita, Japan

Abstract We report an experimental study of the phase diagrams of MgO, $MgSiO_3$, and Mg_2SiO_4 at high pressures. We measured the shock compression response, including pressure-temperature Hugoniot curves of MgO, $MgSiO_3$, and Mg_2SiO_4 between 0.2–1.2 TPa, 0.12–0.5 TPa, and 0.2–0.85 TPa, respectively, using laser-driven decaying shocks. A melting signature has been observed in MgO at 0.47 ± 0.04 TPa and 9860 ± 810 K, while no such phase changes were observed either in $MgSiO_3$ or in Mg_2SiO_4. Increases of reflectivity of MgO, $MgSiO_3$, and Mg_2SiO_4 liquids have been detected above 0.55 TPa (12760 K), 0.15 TPa (7540 K), 0.2 TPa (5800 K), respectively. In contrast to SiO_2, melting and metallization of these compounds do not coincide, implying the presence of poorly electrically conducting liquids close to the melting lines. This has important implications for the generation of dynamos in super-Earth's mantles.

1. Introduction

MgO, $MgSiO_3$, and Mg_2SiO_4 are among the most relevant magnesian end-member components of the Earth's mantle and generally of terrestrial planets. For this reason, detailed knowledge of their phase diagram is essential to properly model interior structures and dynamics of terrestrial planets. However, our comprehension of the processes governing the deeper mantles is limited mainly due to inadequate characterization of magnesium-rich oxide and silicates properties at high pressures. Indeed, thermal profiles of super-Earth's interiors are controlled by the phase transitions of these compounds at even higher pressures [*Stixrude*, 2014]. For example, the core mantle boundary (CMB) in GJ876d, a super Earth with 7.5 Earth masses, is expected to be seated at ~1000 GPa [*Valencia et al.*, 2006] and the temperature at the CMB is assumed to be controlled by the melting curve of mantle components [*Stixrude*, 2014; *Gaidos et al.*, 2010]. Experimental data between 100 and 1000 GPa are thus needed to well constrain melting lines of mantle components and thus Earth-like and super-Earth's CMB conditions [*Du and Lee*, 2014]. Moreover, thermal and transport properties of these compounds at high pressures are also necessary to comprehend planetary evolution and macroscopic characteristics. For example, the metallization of liquid silicates under extreme conditions would promote part of the mantle to a potential magnetic field generator [*Ziegler and Stegman*, 2013; *McWilliams et al.*, 2012; *Millot et al.*, 2015]. It is therefore a strong requirement to study these mineral phase diagrams over a wider pressure and temperature range. In this context dynamic compression is the only available technique to study such high pressure-temperature (*P-T*) conditions. Various theoretical and few experimental studies have lately been carried on dynamically compressed MgO, $MgSiO_3$, and Mg_2SiO_4 phases, but some controversies are not solved yet.

Calculations [*Oganov et al.*, 2003; *Wu et al.*, 2008; *Cebulla and Redmer*, 2014; *Boates and Bonev*, 2013; *Miyanishi et al.*, 2015] and experiments [*Zerr and Boehler*, 1993; *Coppari et al.*, 2013] agree that MgO phase diagram is composed by two solid crystalline phases (with B1 and B2 structures) and a liquid phase. However, at high pressure, phase boundary positions in the *P-T* diagram remain uncertain. Recent decaying [*McWilliams et al.*, 2012] and steady [*Miyanishi et al.*, 2015; *Root et al.*, 2015] shock experiments claim to have observed signatures of melting and of the B1-B2 transitions, but at discordant *P-T* conditions. Furthermore, *McWilliams et al.* [2012] observed that along the Hugoniot, MgO melts directly into a metallic liquid, suggesting that MgO melt could play an important role in magnetic field generation in terrestrial planets. Moreover, the B1-B2 phase transition strongly affects super-Earth mantle rheological properties [*Karato*, 2011] with implications for orbital and thermal evolutions.

Concerning the $MgSiO_3$ phase diagram, below the melting line calculations predict two solid phases with perovskite and postperovskite structures. In the $MgSiO_3$ melt region, a peculiar liquid-liquid phase transition has been observed in decaying shocks experiments, from both glass and single-crystal starting materials [*Spaulding et al*., 2012]. However, either this transition is not predicted [*Militzer*, 2013] or its nature is contested [*Boates and Bonev*, 2013]. This controversy together with the strong implications that a liquid-liquid transition would have for planetary interiors (through geochemical differentiation [*Spaulding et al*., 2012]) encourages deeper investigations.

A few data exist on the Mg_2SiO_4 phase diagram. Indeed, it has been explored with shock compression up to 200 GPa by *Mosenfelder et al*. [2007], *Lyzenga and Ahrens* [1980], and *Luo et al*. [2004], and at higher pressures by *Sekine et al.* [2016] very recently. Sekine et al. claimed that forsterite melt displays a partial phase separation of MgO crystallites, phase transition of the high pressure MgO, and remelting. It is based on the Hugoniot measurements (referred on the quartz Hugoniot data) and thermodynamic analyses of temperature measurements.

Decaying shocks are an efficient method to study phase transitions in transparent materials. A reflecting and not sustained shock is launched into an initially transparent material. Its propagation is monitored measuring time evolutions of thermal emission, shock velocity, and optical reflectivity at the shock front. As the shock is not sustained, the pressure, temperature, and shock velocity gradually decrease in time, following the Hugoniot curve. Phase transition may exhibit strong variations in temperature and/or in shock speed due to release of latent heat or to strong volume change. To detect these variations with optical diagnostics, the release of latent heat or the volume change must be large enough to produce observable imprints on the measured histories and need precise measurements. Moreover, the transition kinetics must be fast enough to occur before the shock front has propagated over distances exceeding the optical depth.

We performed experiments exploring MgO, $MgSiO_3$, and Mg_2SiO_4 with decaying shocks. Our results require a reinterpretation of the behavior of these compounds along the Hugoniot.

2. Materials and Methods

We conducted experimental campaigns on the LULI (Ecole Polytechnique, France) and GEKKO (Institute of Laser Engineering ILE, Osaka University, Japan) laser facilities.

At LULI we used as the drive two frequency-doubled laser beams (wavelength = 0.532 μm) with a 1.2–1.5 ns pulse duration delivering up to 750 J. The focal spot was spatially smoothed with Hybrid Phase Plates resulting in a flat intensity profile of 600 μm diameter. Similarly, at ILE, we used six to nine beams of 2.5 ns at 0.351 μm focused with a Kinoform Phase Plate to 600 μm focal spot diameter. At ILE the total energy was $\leq$ 900 J. Due to the using of the phase plates, only a fraction of the energy irradiates the target. To determine laser intensities on target, we performed hydrodynamical simulations tuning the laser intensity in order to reproduce measurements of the shock velocity in a well-known material (e.g., SiO_2). The laser intensities irradiated on target were varied between 1 and 9×10^{13} W/cm^2.

Targets were made of multilayer pushers glued on 350 μm thick samples: MgO single-crystal, Mg_2SiO_4 single-crystal, and $MgSiO_3$ glass (supporting information).

The choice of pushers is critical in decaying shocks experiments. Indeed, the occurrence of any preheating issued from X-ray emission from coronal plasma and of reverberation waves can affect shock velocity and thermal emission signals, whose interpretation then becomes extremely complicated. To reduce the problem of preheating, we used a low-Z plastic polymer ablator followed by a high-Z X-ray absorbing layer (Au or Fe). Reverberation waves are produced at interfaces with a high impedance mismatch (e.g., CH-Au). Problems arise when the reverberation catches the measured shock in the sample material, producing a jump in

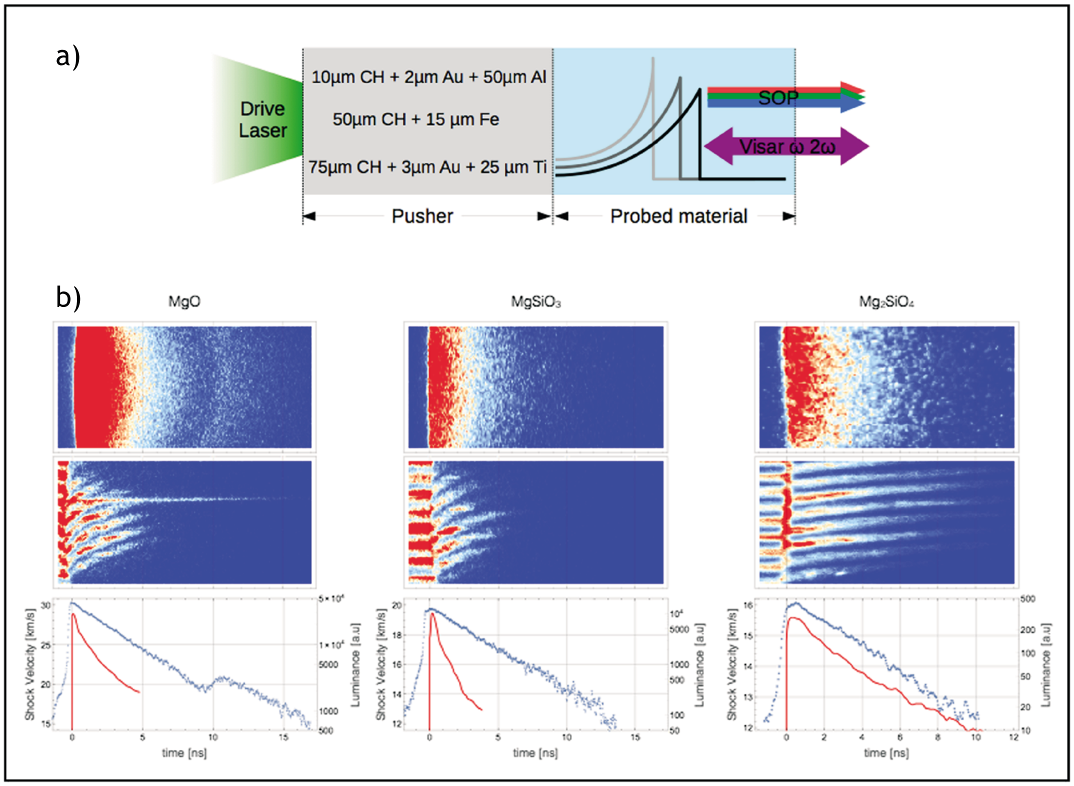

Figure 1. (a) Schematic of experiments and multilayer target. The shock generated into the pusher propagates into the material (MgO, $MgSiO_3$, or Mg_2SiO_4). U_s and reflectivity are measured by VISARs (532 and 1064 nm). Thermal emission is measured by an SOP. (b) Typical SOP and VISAR signals are shown with thermal emission (blue dots) and U_s (red line) time profiles for each material. The represented shots were performed with a 1.2 ns pulse with 726.7 J and 236 J for MgO and $MgSiO_3$, respectively, and with a 2.5 ns pulse with 990 J Mg_2SiO_4.

velocity and temperature signals that might be interpreted as a phase transition (supporting information). We optimized the pusher to avoid this problem. In particular, we tested three different types of pusher (Figure 1a): (i) 10 μm CH/2 μm Au/50 μm Al; (ii) 50 μm CH/15 μm Fe; and (iii) 75 μm CH/3 μm Au/25 μm Ti.

A study conducted on SiO_2 as a reference material allowed us to establish that pushers 2 and 3 are suitable for our measurements, while pusher 1 is not appropriate for decaying shock on thick samples (supporting information).

The two main diagnostics were VISAR (velocity interferometer system for any reflector) [*Celliers et al.*, 2004] at two wavelengths (532 and 1064 nm) and a streaked optical pyrometer (SOP). VISARs allow to precisely measure shock velocity (U_s) and reflectivity as function of time with sensitivities described in supporting information.

In order to extract pressures (P) from U_s measurements we used interpolation of experimental data from literature and/or theoretical models of equation of state (EoS) (supporting information): (i) *Root et al.* [2015] and Mie-Grüneisen-Debye for MgO [*McWilliams et al.*, 2012]; (ii) *Spaulding et al.* [2012] and QEOS [*More et al.*, 1988] for $MgSiO_3$; (iii) QEOS [*More et al.*, 1988] for Mg_2SiO_4.

The calibrated SOP diagnostic (supporting information) coupled to reflectivity data allows us to calculate temperature using the grey body emission hypothesis.

3. Results

3.1. MgO

MgO shock velocity (U_s) and thermal emission are shown in Figure 1b. While U_s decays monotonically, the thermal emission profile exhibits a clear "bump" (at ~11 ns for the shot shown in Figure 1b). The

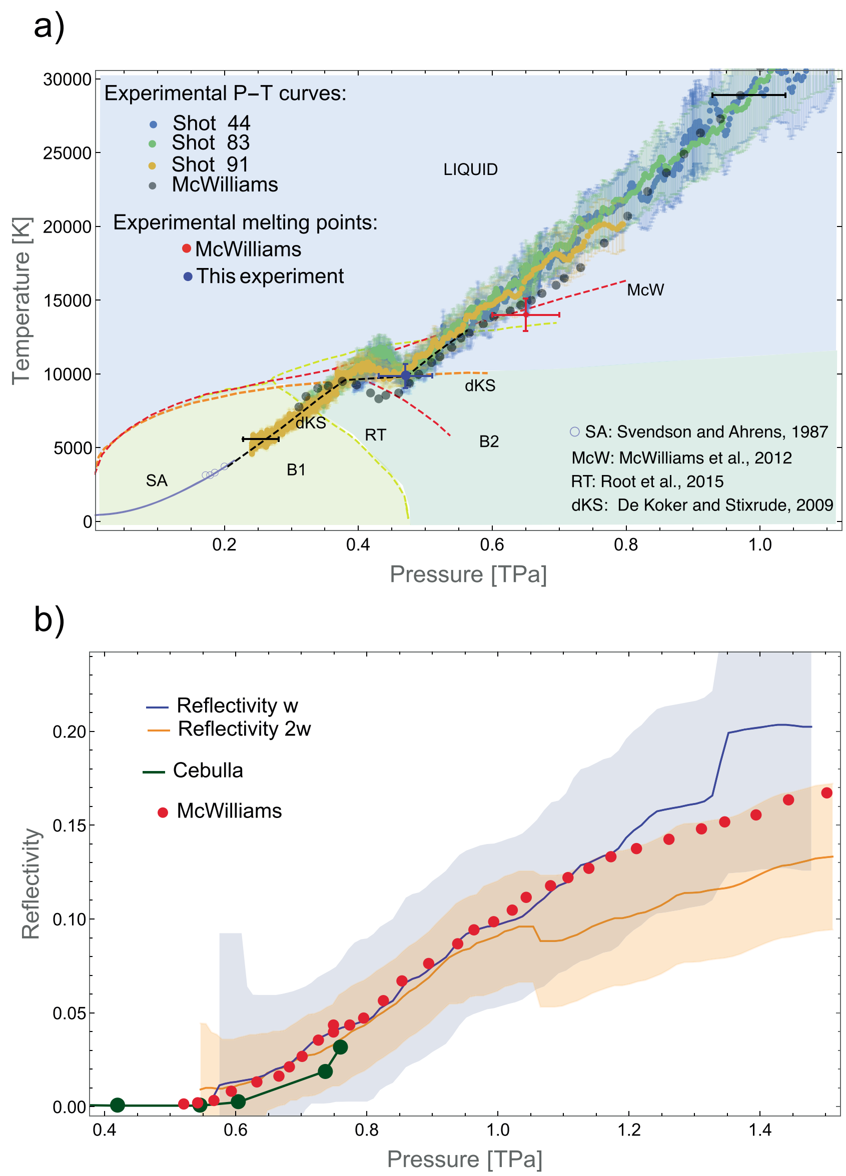

Figure 2. (a) Experimental *P-T* curves measured along the Hugoniot at LULI (colored dots) represented in the MgO *P-T* diagram in comparison with previous experimental and theoretical *P-T* curves (black dots for *McWilliams et al.* [2012], black dashed line dKS for *De Koker and Stixrude* [2009], and blue line SA for *Svendson and Ahrens* [1987]) and phase boundaries (McW is for *McWilliams et al.* [2012], orange line dKS is for *De Koker and Stixrude* [2009], and yellow line RT is for *Root et al.* [2015]). Blue circles are steady shock measurements by *Svendson and Ahrens* [1987]. Black horizontal bars represent the error on pressure in present measurements. (b) MgO reflectivity lines at 532 nm (orange) and at 1064 nm (blue), in comparison with previous experimental results (red dots) [*McWilliams et al.*, 2012] and calculations (green dots) [*Cebulla and Redmer*, 2014].

thermodynamic conditions associated to this incident cannot be directly inferred from optical data since it occurs in a nonreflecting regime and U_s cannot be measured (fringes disappear in Figure 1b). Therefore, U_s to be associated with thermal emission in this regime is obtained using extrapolation methods, as presented in the supporting information of *McWilliams et al.* [2012]. The corresponding *P-T* curves are shown in Figure 2a.

We underline that shocks generated with different laser pulses reproduce the bump at the same *P-T* conditions. As examples, Figure 2a shows shots 91, 44, and 83 performed, respectively, with a 1.2 ns laser pulse of 265, 448.6, and 726.7 J on target type 2. This implies that the bump is a phase transition signature, and it is not produced by reverberating waves. Indeed, in the latter case, for different laser conditions, the bump would be expected to occur at different pressures depending on the dynamic of the shock (velocity and decay rate). Moreover, the curvatures of our thermal emission SOP data are typical of phase transition [*Millot*, 2016].

Since recent calculations [*Oganov et al*., 2003; *Wu et al*., 2008; *Cebulla and Redmer*, 2014; *Miyanishi et al*., 2015; *Root et al*., 2015] agree on the prediction that the Hugoniot curve crosses melting and B1-B2 lines, we interpret the bump as a signature of the melting of the B2 phase. This interpretation is based on different arguments. First, recent ab initio simulations predict an important discontinuity along the Hugoniot at the B2 melting in a pressure interval $\Delta P \sim 120$ GPa against $\Delta P \sim 40$ GPa at the B1/B2 boundary [*Miyanishi et al*., 2015; *Root et al*., 2015]. As a shock can follow a thermodynamic path out of equilibrium (which is our case, as explained below), we do not expect to reproduce exactly the ΔP calculated at equilibrium but to have a more pronounced signature for melting than for the B1/B2 transition. Second, we observed that changing laser intensities, and thus decay dynamics, bump amplitudes changed (Figure S8), supporting the idea of a nonequilibrium phenomenon. Moreover, the bump shape is typical of superheating [*Luo and Ahrens*, 2004]. We underline that a decaying shock experiment is equivalent to a series of dynamic compressions of successively weaker shock strengths. This means that during the shock propagation different sample layers are compressed and heated from the same initial cold state. Features similar to the one we measured were attributed to superheating in previous laser and gas-gun experiments on alpha quartz, stishovite, and fused silica [*Lyzenga et al*., 1983; *Hicks et al*., 2006; *Millot et al*., 2015]. Third, to investigate the possibility to detect the B1/B2 transition, we performed ab initio calculations estimating the MgO optical depth. The calculated optical depth is $>10\ \mu$m at ~ 325 GPa (i.e., around the B1/B2 expected transition) whereas it is $<1\ \mu$m close to the melting point (470 GPa) detected here. In the first case, the thermal emission comes not only from the shock front but from a 10 μm inhomogeneous region behind it, which exhibits roughly uniform temperature but a pressure variation of 30 GPa (supporting information). Thus, since the measured signal results from the integration of the light coming from this inhomogeneous region, whether a phase transition occurs its signature could be smoothed. In addition the SOP noise is higher at lower *P-T* conditions. Hence, the thermal emission data in these thermodynamic states are not suitable for a reliable phase transition detection along the Hugoniot. Nevertheless, we still believe the data between 325 and 240 GPa to be representative of the *P-T* Hugoniot curve, considering the uncertainty of ~ 30 GPa given by the pressure variation in the probed volume. This reliability seems to be confirmed by the good agreement with previous theoretical [*Svendson and Ahrens*, 1987; *De Koker and Stixrude*, 2009] and experimental works [*Svendson and Ahrens*, 1987]. To conclude this point, we think that the detection of B1/B2 has been missed mainly because of the small discontinuity predicted for this transition (according to theory [*Cebulla and Redmer*, 2014; *Miyanishi et al*., 2015; *Root et al*., 2015]). The smoothing effect mentioned above could have played an additional role.

We therefore interpret the “bump” as superheated melting signature of the B2 phase. In the occurrence of superheating, the melting line is tangent to the minimum of the observed feature [*Luo and Ahrens*, 2004] and the melting point corresponds to the “bump” minimum. Nevertheless, a different scenario where the Hugoniot would cross liquid/B1 boundary, skipping the B2 phase, cannot be excluded. Direct structural investigations using in situ X-ray diffraction will be mandatory to resolve this issue.

Our measurements on MgO highlight a melting point at 0.47 ± 0.04 TPa and 9860 ± 810 K (0.85 ± 0.07 eV). This interpretation is partially in contrast with previous experimental results [*McWilliams et al*., 2012], where melting was determined at 0.65 ± 0.05 TPa and $14{,}000 \pm 1100$ K along the Hugoniot, as inferred from a slope change in the *P-T* curve (pointed by the red cross in Figure 2a). Furthermore, *McWilliams et al.* [2012] interpreted a feature at 0.44 ± 0.08 TPa and 9000 ± 700 K as a signature of the B1-B2 transition. However, while the *McWilliams et al.* [2012] results are well fitted only by calculations by *Boates and Bonev* [2013], our interpretation is supported by the majority of the most recent ab initio calculations [*Oganov et al*., 2003; *Wu et al*., 2008; *Cebulla and Redmer*, 2014; *Miyanishi et al*., 2015; *Root et al*., 2015] which predicts the melting line to pass through 0.47 TPa at ~11,750 K [*Root et al*., 2015; *Miyanishi et al*., 2015] and the B1-B2 coexistence line to lie ~150 GPa lower than *McWilliams et al.* [2012]. Hence, our experimental melting point agrees with lower melting lines [e.g., *De Koker and Stixrude*, 2009] than *McWilliams et al.* [2012] implying a lowering of super-Earths’ temperature profile [*Stixrude*, 2014; *Gaidos et al*., 2010]. Reflectivity data (Figure 2b) have important implications, too. Indeed, reflectivities start to smoothly increase at ~ 0.55 TPa, i.e., at higher pressures than the measured melting point (at 0.47 TPa and 9860 K), suggesting that melting

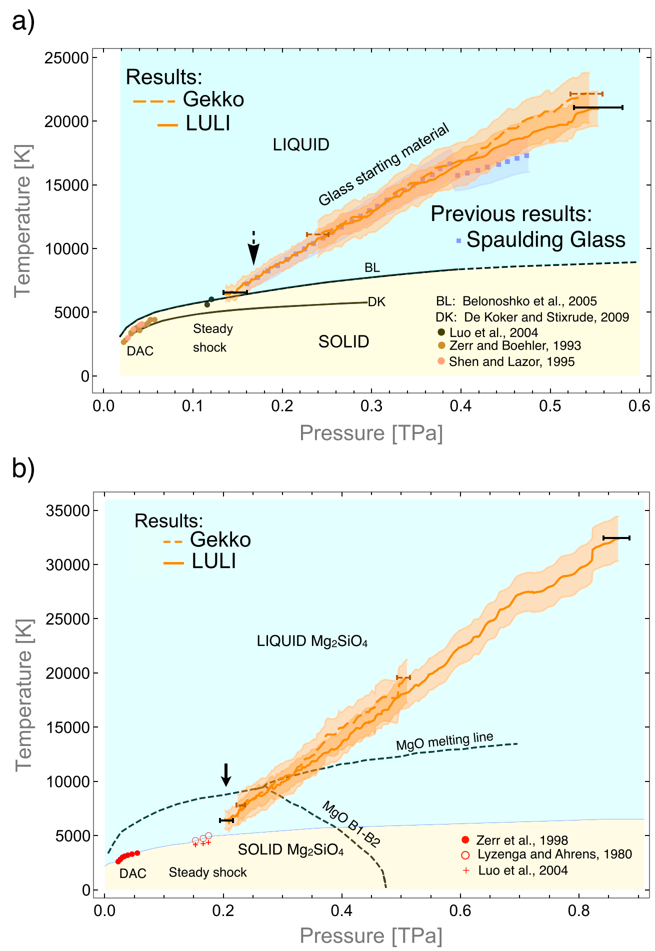

Figure 3. (a) Experimental $MgSiO_3$ glass *P-T* curves measured along the Hugoniot at LULI (orange full line) and at Gekko (dotted orange line) in comparison with previous experimental results ([*Spaulding et al.*, 2012] blue square). Black dots represent steady shock measurements [*Luo et al.*, 2004]. Pink and brown dots show diamonds anvil cell (DAC) melting measurements [*Shen and Lazor*, 1995] and [*Zerr and Boehler*, 1993], respectively. Black lines represent theoretical melting lines (BL is *Belonoshko et al.* [2005] and DK is *De Koker and Stixrude* [2009]). (b) Experimental Mg_2SiO_4 *P-T* curves measured at LULI (orange full line) and at Gekko (dotted orange line). Red dots represent DAC melting measurements [*Zerr et al.*, 1998]. Red circles and crosses represent steady shock data measured by *Lyzenga and Ahrens* [1980] and corrected values by *Luo et al.* [2004], respectively (*Mosenfelder et al.* [2007] did not measure temperatures). Dashed lines show MgO coexistence lines from *Root et al.* [2015]. Black and brown dashed horizontal bars represent the error on pressure for LULI and Gekko data, respectively, for both materials. The arrows indicate the beginning of the reflecting segment along the Hugoniot.

is not directly associated with metallisation. Moreover, between 0.55 and 1 TPa, the reflectivity at 532 nm ($R(2\omega)$) is similar to the reflectivity at 1064 nm ($R(\omega)$), while for pressures higher than 1 TPa $R(\omega) > R(2\omega)$, saturating at ~20% and ~13%, respectively. This behavior suggests a transition from a "semiconductor" to a metal. To calculate conductivities, we applied two different models according to the pressure regime. At low pressures (corresponding to the region where reflectivity starts to increase) we applied a Drude-semiconductor model [*McWilliams et al.*, 2012; *Hicks et al.*, 2006] and we found a conductivity ~10^4 S/m for 1% reflectivity [*McWilliams et al.*, 2012]. At 1.4 TPa instead (where reflectivities suggest a metallic behavior), taking advantage from our two wavelength reflectivity measurements, we applied the Drude free-electron model [*Goettel et al.*, 1989], finding at 1.4 TPa a DC conductivity of 1.3×10^5 S/m and a scattering time of 1.3×10^{-17} s. This means that along the Hugoniot between 0.47 and ~0.55 TPa, MgO liquid has a conductivity $<10^4$ S/m and ~10^3 S/m at 0.47 TPa using extrapolation of the Drude-semiconductor model [*McWilliams et al.*, 2012]. These results are confirmed by more sophisticated ab initio calculations, which predict ~7×10^4 S/m for a 2% reflectivity. Such low conductivities are close to the minimum value for the dynamo mechanism to be operating in a molten layer at the bottom of a silicate mantle [*Ziegler and Stegman*, 2013]. This result is an important input for evaluating liquid MgO contribution to the planetary magnetic field generation.

3.2. $MgSiO_3$

$MgSiO_3$ thermal emission at the shock front decreases exponentially with U_s exhibiting the typical behavior for a material without any distinct phase transition. Indeed, for $MgSiO_3$ glass, we have not observed any bumps, in contrast to a recent decaying shock experiment where a liquid-liquid phase transition was detected [*Spaulding et al.*, 2012] and with recent ab initio calculations that predict a demixing transition [*Umemoto et al.*, 2006; *Boates and Bonev*, 2013]. $MgSiO_3$ glass *P-T* curves along the Hugoniot obtained at LULI and GEKKO are shown in Figure 3a. Since our shocks start propagating in the melt region of the phase diagram [*Shen and Lazor*, 1995; *Belonoshko et al*., 2005; *De Koker and Stixrude*, 2009], the most likely interpretation from our data is that the shocks propagated through one single liquid phase. We strengthen our result with some considerations. First, we expect that in our targets, no hydrodynamic effects could have affected shock decays [*Supporting information*]. Moreover, our results have been reproduced at two different facilities (LULI2000 and GEKKO). Furthermore, below 0.4 TPa our Hugoniot data are in agreement with *Spaulding et al.* [2012]. The only disagreement concerns the feature at 0.4 TPa that has been proposed as a liquid-liquid phase transition by *Spaulding et al.* [2012]. However, we remark that liquid-liquid transitions are rare (occurring, e.g., in liquid phosphorous [*Katayama et al*., 2000]) and that for $MgSiO_3$ this phase transitions has not been reproduced by molecular dynamics calculations [*Militzer,* 2013]. Our data do not confirm the presence of dissociation, predicted, with different phase boundaries, by *Boates and Bonev* [2013] and *Umemoto et al.* [2006]. Furthermore, our *P-T* curve is consistent with low-pressure steady shock data [*Luo et al*., 2004]. Our data set does not rule out gradual changes in Si coordination number by oxygen under extreme pressure or other structural transitions in the liquid state, but it implies that their effects on decaying shock would be too weak to produce distinct features in the data.

The reflectivity has been observed to increase above 0.15 TPa as pointed by the arrow in Figure 3a. The absence of transition signature until the detection limit suggests to set an upper limit for melting at 6300 ± 690 K at 0.12 TPa, which unfortunately does not allow to discriminate between the melting lines calculated by *Belonoshko et al.* [2005] and *De Koker and Stixrude* [2009]. Again, melting and reflectivity increases are not coincident, suggesting the presence of a poorly conducting liquid also in the $MgSiO_3$ high-pressure phase diagram.

3.3. Mg_2SiO_4

The high-pressure phase diagram of Mg_2SiO_4 is poorly known beyond 200 GPa. Only a few Hugoniot measurements [*Sekine et al*., 2016] exist. In particular, it is not well defined whether forsterite breaks down into MgO-$MgSiO_3$-MgO-SiO_2 systems or melts into pure Mg_2SiO_4 [*Mosenfelder et al*., 2007; *De Koker et al*., 2008]. Hence, for Mg_2SiO_4, we looked both for any signatures of dissociation or melting, along the Hugoniot, as well as for any evidence of crystalline MgO at the crossing between the Hugoniot and MgO phase boundaries. We obtained the pressure/temperature curves shown in Figure 3b, where the shock pressure decays monotonically between 850 and 200 GPa. In this region neither velocity nor emission profiles exhibit signatures of phase transitions. Moreover, no features have been observed at the crossing between the Hugoniot and MgO phase boundaries. In particular, the data do not show the melting signature detected at 0.47 TPa and 9860 K in MgO samples. These results either exclude the presence of crystalline MgO below its melt curve (i.e., Mg_2SiO_4 remains in a single undissociated phase, potentially because of the slow dissociation kinetic) or suggest that because of an eutectic behavior in the MgO-SiO_2 or MgO-$MgSiO_3$ system, MgO concentration is not high enough to generate a detectable signature with decaying shocks. This conclusion contradicts what recently found [*Sekine et al*., 2016]. To investigate this discrepancy, we carefully compared our raw data with those of Sekine et al. (their Table 1). The results are in agreement within error bars except for one single point at 344 GPa (Figure S11), which is the datum leading to the interpretation of phase transition of MgO. The origin of this difference calls for further EoS shock experiments to test the reproducibility of these data and increase the sampling of this crucial region of the phase diagram.

We observed Mg_2SiO_4 reflectivity starting to increase at 0.2 TPa. No melting signatures have been detected down to 0.2 TPa and 6300 ± 680 K (SOP detection limit), in agreement with previous works [*Lyzenga and Ahrens*, 1980; *Luo and Ahrens*, 2004] which set forsterite melting between 150 GPa and 170 GPa along the Hugoniot. Our data underline that as for MgO and $MgSiO_3$, melting does not coincide with the onset of reflectivity, suggesting the existence of a poorly conductive liquid in the Mg_2SiO_4 high-pressure phase diagram.

4. Conclusions

In this study, we obtained pressure-temperature measurements along the Hugoniot of different compounds in the MgO-SiO_2 chemical system.

We propose an upper limit of the MgO melting point at 0.47 ± 0.04 TPa and 9860 ± 810 K (0.85 ± 0.07 eV). This is lower than several estimates of melting in this pressure range, and it implies lower temperature profiles for Earth-like planets and super-Earths [*Stixrude*, 2014; *Gaidos et al*., 2010]. As iron should be present in planetary mantles, future experiments on FeO and (Mg, Fe)O should be conducted in order to constrain partial melting conditions in this system. Moreover, molten MgO could play an important role in the case of deep magma oceans and/or in response to very large impacts, as well as in the putative cores of icy giant and gas giant planets (as for tidal dissipation [*Remus et al.*, 2012]). The scenario proposed here with a lower temperature melting curve brings a new important input for modeling studies of these phenomena.

We showed that no detectable phase transition could be observed either in $MgSiO_3$ or in Mg_2SiO_4 in the range (0.12 TPa-6300 K, 0.5 TPa-22,000 K) and (0.2 TPa-6300 K, 0.8 TPa-30,000 K), respectively. This result is in disagreement with previous experimental data [*Spaulding et al.*, 2012] and calls for a novel interpretation of the behavior of high-pressure silicate liquids. In particular, it excludes a role of the liquid-liquid transition in planetary geochemical differentiation, with consequences for the bulk chemical composition of significant fractions of a planet in its early stages [*Spaulding et al.*, 2012]. In addition, no signature of the occurrence of crystalline MgO could be detected in both $MgSiO_3$ and Mg_2SiO_4 data sets. Several hypotheses have been proposed to explain these observations, including the stability of undissociated $MgSiO_3$ and Mg_2SiO_4 liquids. Nevertheless, due to the importance of this debate, further direct structural investigations under dynamic compression are mandatory.

Interestingly, for all the studied materials, we observed that metallization and melting do not occur at coincident thermodynamic conditions (reflectivity starts to increase at *P-T* along the Hugoniot higher than melting), implying the presence of poorly electrically conducting liquid in the melting line vicinity. This result is extremely relevant for the models of magnetic field generation via dynamo mechanism in a molten silicate layer, where a strongly conducting liquid is necessary to sustain the magnetic field. In addition, this behavior is different to what was established for SiO_2 (where along the Hugoniot reflectivity starts to increase at melting) [*Spaulding Thesis*; *Hicks et al.*, 2006], pointing out a difference in the electronic structure changes at melting between MgO, $MgSiO_3$, and Mg_2SiO_4 on one hand and SiO_2 on the other. This intriguing input for condensed matter studies encourages deeper investigations of the high-pressure regime of these materials with X-ray diagnostics.

Altogether, these results enable a new interpretation of magnesium oxides phase diagrams at extreme conditions that need to be accounted for when modeling super-Earths. During super-Earths evolution, the studied liquids may not show structural transitions and will be poor electrical conductors close to the melting line. The different parameters presented in our study will be important inputs to model super-Earths' dynamics, internal structure, and evolution.

Acknowledgments
This research was supported by the PlanetLab program of the Agence Nationale de la Recherche (ANR) grant ANR-12-BS04-0015-04. Discussions with V. Recoules have been very helpful for ab initio calculations. We would like to thank Mélanie Escudier (INSP, Paris 6 University) for her careful and precious help during polishing and preparation of the starting materials. We would like also to thank Laurent Cormier (IMPMC, Paris 6 University) for the synthesis of $MgSiO_3$ glass in high temperature furnace. Laser shock experiments were conducted under the joint research project of the Institute of Laser Engineering, Osaka University. This work was supported in part by JSPS KAKENHI grant 15K13609, JSPS core to core program on International Alliance for Material Science in Extreme States with High Power Laser and XFEL, and the X-ray Free Electron Laser Priority Strategy Program at Osaka University from the Ministry of Education, Culture, Sports, Science and Technology (MEXT). This experiment has been performed thanks to collaborations supported by GDRI N° 118 MECMA TPLA. We acknowledge the support of the COST Action MP1208 "developing the physics and the scientific community for inertial fusion." Measured temperature-shock velocity curves are reported in the supporting information. Original VISAR and SOP data used are archived in the Gekko and LULI repositories and are available from the authors upon request according to the AGU data policy.

References

Belonoshko, A. B., N. V. Skorodumova, A. Rosengren, R. Ahuja, B. Johansson, L. Burakovsky, and D. L. Preston (2005), High-pressure melting of $MgSiO_3$, *Phys. Rev. Lett.*, *94*(19), 20–23, doi:10.1103/PhysRevLett.94.195701.

Boates, B., and S. A. Bonev (2013), Demixing instability in dense molten $MgSiO_3$ and the phase diagram of MgO, *Phys. Rev. Lett.*, *110*(13), 1–5, doi:10.1103/PhysRevLett.110.135504.

Cebulla, D., and R. Redmer (2014), Ab initio simulations of MgO under extreme conditions, *Phys. Rev. B*, *89*(13), 134107, doi:10.1103/PhysRevB.89.134107.

Celliers, P. M., D. K. Bradley, G. W. Collins, D. G. Hicks, T. R. Boehly, and W. J. Armstrong (2004), Line-imaging velocimeter for shock diagnostics at the OMEGA laser facility, *Rev. Sci. Instrum.*, *75*(11), 4916–4929, doi:10.1063/1.1807008.

Coppari, F., R. F. Smith, J. H. Eggert, J. Wang, J. R. Rygg, A. Lazicki, J. A. Hawreliak, G. W. Collins, and T. S. Duffy (2013), Experimental evidence for a phase transition of magnesium oxide at exoplanet pressures, *Nat. Geosci.*, *6*(11), 926, doi:10.1038/NGEO1948.

de Koker, N., and L. Stixrude (2009), Self-consistent thermodynamic description of silicate liquids, with application to shock melting of MgO periclase and $MgSiO_3$ perovskite, *Geophys. J. Int.*, *178*(1), 162–179, doi:10.1111/j.1365-246X.2009.04142.x.

de Koker, N. P., L. Stixrude, and B. B. Karki (2008), Thermodynamics, structure, dynamics, and freezing of Mg_2SiO_4 liquid at high pressure, *Geochim. Cosmochim. Acta*, *72*(5), 1427–1441, doi:10.1016/j.gca.2007.12.019.

Du, Z., and K. K. M. Lee (2014), High-pressure melting of MgO from (Mg,Fe)O solid solutions, *Geophys. Res. Lett.*, *41*, 8061–8066, doi:10.1002/2014GL061954.

Gaidos, E., C. P. Conrad, M. Manga, and J. Hernlund (2010), Thermodynamic limits on magnetodynamos in rocky exoplanets, *Astrophys. J.*, *718*, 596–609, doi:10.1088/0004-637X/718/2/596.

Goettel, K. A., J. H. Eggert, and I. F. Silvera (1989), Optical evidence for the metallization of Xenon at 132(5) GPa, *Phys. Rev. Lett.*, *62*(6), 665–668, doi:10.1103/PhysRevLett.62.665.

Gonze, X., et al. (2009), ABINIT: First-principles approach to material and nanosystem properties, *Comput. Phys. Commun.*, *180*(12), 2582–2615, doi:10.1016/j.cpc.2009.07.007.

Hicks, D. G., T. R. Boehly, J. H. Eggert, J. E. Miller, P. M. Celliers, and G. W. Collins (2006), Dissociation of liquid silica at high pressures and temperatures, *Phys. Rev. Lett.*, *97*(2), 3–6, doi:10.1103/PhysRevLett.97.025502.

Karato, S. (2011), Rheological structure of the mantle of a super-Earth: Some insights from mineral physics, *Icarus*, *212*(1), 14–23, doi:10.1016/j.icarus.2010.12.005.

Katayama, Y., T. Mizutani, W. Utsumi, O. Shimomura, M. Yamakata, and K. Funakoshi (2000), A first-order liquid-liquid phase transition in phosphorus, *Nature*, *403*(6766), 170–173, doi:10.1038/35003143.

Luo, S. N., and T. J. Ahrens (2004), Shock-induced superheating and melting curves of geophysically important minerals, *Phys. Earth Planet. Inter.*, *143*(1–2), 369–386, doi:10.1016/j.pepi.2003.04.001.

Luo, S. N., J. A. Akins, T. J. Ahrens, and P. D. Asimow (2004), Shock-compressed $MgSiO_3$ glass, enstatite, olivine, and quartz: Optical emission, temperatures, and melting, *J. Geophys. Res.*, *109*, B05205, doi:10.1029/2003JB002860.

Lyzenga, G. A., and T. J. Ahrens (1980), Shock temperature measurements in $Mg2SiO_4$ and SiO_2 at high pressures, *Geophys. Res. Lett.*, *7*, 141–144, doi:10.1029/GL007i002p00141.

Lyzenga, G. A., T. J. Ahrens, and A. C. Mitchell (1983), Shock temperatures of SiO_2 and their geophysical implications, *J. Geophys. Res.*, *88*, 2431–2444, doi:10.1029/JB088iB03p02431.

Mazevet, S., M. Torrent, V. Recoules, and F. Jollet (2010), Calculations of the transport properties within the PAW formalism, *High Energy Density Phys.*, *6*(1), 84–88, doi:10.1016/j.hedp.2009.06.004.

McWilliams, S., D. Spaulding, J. H. Eggert, P. Celliers, D. G. Hicks, R. F. Smith, G. W. Collins, and R. Jeanloz (2012), Phase transformations and metallization of magnesium oxide at high pressure and temperature, *Science*, *338*, 1330–1333.

Militzer, B. (2013), Ab initio investigation of a possible liquid-liquid phase transition in $MgSiO_3$ at megabar pressures, *High Energy Density Phys.*, *9*(1), 152–157, doi:10.1016/j.hedp.2012.11.006.

Miller, J. E., T. R. Boehly, A. Melchior, D. D. Meyerhofer, P. M. Celliers, J. H. Eggert, D. G. Hicks, C. M. Sorce, J. A. Oertel, and P. M. Emmel (2007), Streaked optical pyrometer system for laser-driven shock-wave experiments on OMEGA, *Rev. Sci. Instrum.*, *78*(3), 034903, doi:10.1063/1.2712189.

Millot, M., N. A. Dubrovinskaia, A. Cernok, S. Blaha, L. S. Dubrovinsky, D. G. Braun, P. M. Celliers, G. W. Collins, J. H. Eggert, and R. Jeanloz (2015), Shock compression of stishovite and melting of silica at planetary interior conditions, *Science*, *347*(6220), 418, doi:10.1126/science.1261507.

Millot, M. N. (2016), Identifying and discriminating phase transitions along decaying shocks with line imaging Doppler interferometric velocimetry and streaked optical pyrometry, *Phys. Plasmas*, *23*(1), 014503, doi:10.1063/1.4940942.

Miyanishi, K., Y. Tange, N. Ozaki, T. Kimura, T. Sano, Y. Sakawa, T. Tsuchiya, and R. Kodama (2015), Laser-shock compression of magnesium oxide in the warm-dense-matter regime, *Phys. Rev. E: Stat., Nonlinear, Soft Matter Phys.*, *92*(2), 1–5, doi:10.1103/PhysRevE.92.023103.

More, R. M., K. Warren, D. A. Young, and G. Zimmerman (1988), A new quotidian equation of state (QEOS) for hot dense matter, *Phys. Fluids*, *31*(10), 3059, doi:10.1063/1.866963.

Mosenfelder, J. L., P. D. Asimow, and T. J. Ahrens (2007), Thermodynamic properties of Mg_2SiO_4 liquid at ultra-high pressures from shock measurements to 200 GPa on forsterite and wadsleyite, *J. Geophys. Res.*, *112*, B06208, doi:10.1029/2006JB004364.

Oganov, A. R., M. J. Gillan, and G. D. Price (2003), Ab initio lattice dynamics and structural stability of MgO, *J. Chem. Phys.*, *118*(22), 10,174–10,182, doi:10.1063/1.1570394.

Ramis, R., R. Schmalz, and J. Meyer-Ter-Vehn (1988), MULTI: A computer code for one-dimensional multigroup radiation hydrodynamics, *Comput. Phys. Commun.*, *49*(3), 475–505, doi:10.1016/0010-4655(88)90008-2.

Remus, F., S. Mathis, J.-P. Zahn, and V. Lainey (2012), Anelastic tidal dissipation in multi-layer planets, *Astron. Astrophys.*, *541*(A), 165, doi:10.1051/0004-6361/201118595.

Root, S., L. Shulenburger, R. W. Lemke, D. H. Dolan, T. R. Mattsson, and M. P. Desjarlais (2015), Shock response and phase transitions of MgO at planetary impact conditions, *Phys. Rev. Lett.*, *115*(19), 1–6, doi:10.1103/PhysRevLett.115.198501.

Sekine, T., et al. (2016), Shock compression response of forsterite above 250 GPa, *Sci. Adv.*, *2*, e1600157, doi:10.1126/sciadv.1600157.

Shen, G., and P. Lazor (1995), Measurement of melting temperatures of some minerals under lower mantle pressures, *J. Geophys. Res.*, *100*, 17,699–17,713, doi:10.1029/95JB01864.

Spaulding, D. K., R. S. McWilliams, R. Jeanloz, J. H. Eggert, P. M. Celliers, D. G. Hicks, G. W. Collins, and R. F. Smith (2012), Evidence for a phase transition in silicate melt at extreme pressure and temperature conditions, *Phys. Rev. Lett.*, *108*(6), 1–4, doi:10.1103/PhysRevLett.108.065701.

Stephens, R. E., and I. H. Malitson (1952), Index of refraction of magnesium oxide, *J. Res. Natl. Bur. Stand.*, *49*(4), 249, doi:10.6028/jres.049.025.

Stixrude, L. (2014), Melting in super-Earths, *Philos. Trans. R. Soc. A*, *372*, 20130076.

Svendson, B., and T. J. Ahrens (1987), Shock-induced temperatures of MgO, *Geophys. J. R. Astron. Soc.*, *91*, 667–691.

Umemoto, K., R. M. Wentzcovitch, and P. B. Allen (2006), Dissociation of $MgSiO_3$ in the cores of gas giants and terrestrial exoplanets, *Science*, *311*(5763), 983–986, doi:10.1126/science/1120865.

Valencia, D., R. J. O'Connell, and D. Sasselov (2006), Internal structure of massive terrestrial planets, *Icarus*, *181*, 545–554.

Wu, Z., R. M. Wentzcovitch, K. Umemoto, B. Li, K. Hirose, and J. C. Zheng (2008), Pressure-volume-temperature relations in MgO: An ultrahigh pressure-temperature scale for planetary sciences applications, *J. Geophys. Res.*, *113*, B06204, doi:10.1029/2007JB005275.

Zeldovich, Y. B., and Y. P. Raizer (1967), *Physics of Shock Waves and High-Temperature Hydrodynamic Phenomena*, Academic, New York.

Zerr, A., and R. Boehler (1993), Melting of (Mg, Fe)SiO_3-perovskite to 625 kilobars: Indication of a high melting temperature in the lower mantle, *Science*, *262*(5133), 553, doi:10.1126/science.262.5133.553.

Zerr, A., A. Diegeler, and R. Boehler (1998), Solidus of Earth's deep mantle, *Science*, *281*(July), 243–246.

Ziegler, L. B., and D. R. Stegman (2013), Implications of a long-lived basal magma ocean in generating Earth's ancient magnetic field, *Geochem. Geophys. Geosyst.*, *14*, 4735–4742, doi:10.1002/2013GC005001.

Erratum

In the originally published version of this article, the refractive index of $MgSiO_3$ used to perform the analysis (1.66 at 532 nm) was imprecise. Literature reported different and contradictory values. To correct the error, a precise index of refraction ellipsometry measurement was performed and reliable values (1.614 at 532 nm and 1.6 at 1064 nm) were used to correct the analysis. The values have been corrected in the text. Figure 3a in the article and Figure S12 in the supporting information have also been corrected. The present version may be considered the authoritative version of record.